PCCP

Aggregation kinetics of single-walled carbon nanotubes by mechanically wrapped multinuclear complexes: probing the tube – tube repulsive barrier

Journal:	*Physical Chemistry Chemical Physics*
Manuscript ID:	CP-ART-12-2013-055530.R1
Article Type:	Paper
Date Submitted by the Author:	29-Jan-2014

Complete List of Authors:	Ameen, Anjail; University of North Carolina at Charlotte, Chemistry Giordano, Andrea; University of North Carolina at Charlotte, Chemistry Alston, Jeffrey; University of North Carolina at Charlotte, Chemistry Forney, Michael; University of North Carolina at Charlotte, Chemistry Herring, Natalie; University of North Carolina at Charlotte, Chemistry Kobayashi, Shiho; University of North Carolina at Charlotte, Chemistry Ridlen, Shawn; University of North Carolina at Charlotte, Chemistry Subaran, Sarah; University of North Carolina at Charlotte, Chemistry Younts, Thomas; University of North Carolina at Charlotte, Chemistry Poler, Jordan; University of North Carolina at Charlotte, Chemistry

Physical Chemistry Chemical Physics

Aggregation kinetics of single-walled carbon nanotubes by mechanically wrapped multinuclear complexes: probing the tube – tube repulsive barrier

Anjail A. Ameen, [a] Andrea N. Giordano, [a] Jeffrey R. Alston, [a] Michael W. Forney, [a] Natalie P. Herring, [a] Shiho Kobayashi, [a] Shawn G. Ridlen, [a] Sarah S. Subaran, [a] Thomas J. Younts, [a] and J. C. Poler[a†]

[a] Department of Chemistry, University of North Carolina at Charlotte, Charlotte, NC

[a†] Corresponding Author: Department of Chemistry, University of North Carolina at Charlotte, Charlotte, NC Fax: (704) 687-0960; Tel: (704) 687-8289; E-mail: jcpoler@uncc.edu

† Electronic supplementary information (ESI) available: 1. Water determination by NMR, 2. Additional SEM of supraparticle assemblies, 3. Molar conductivities of coagulants, 4. Zeta potential data, 5. Molecular dynamics simulations of SWCNTs in DMF, 6. Schulze-Hardy plot for some coagulants, 7. Molecular dynamics of solvated molecular ion, 8. Kinetics of aggregation data.

Abstract

The rational design of supraparticle assemblies requires detailed understanding of directed assembly processes. The stability of dispersions of nanoscale materials, like single-walled carbon nanotubes (SWCNTs), is still not fully understood, nor are the mechanisms of aggregation and assembly. A detailed balance of attractive van der Waals type interactions with various repulsive barrier mechanisms is needed to control the assembly of industrial-viable and functional hybrid-nanoscale supraparticles. We are reporting a detailed study of SWCNT dispersion stability and aggregation kinetics as a function of the nature of the coagulant used in various solvent systems. We explore three classes of coagulants that vary by charge, size, shape, solvation energy, and ability to bind to the SWCNTs. We use these kinetic data to assess the tube-solvent-coagulant-tube interactions. We compare the relative contributions from two types of repulsive barriers. We find that tube-mediated structured solvent around the SWCNTs does not sufficiently describe our measured kinetic data. A DLVO type, electrical double layer repulsion is used to rationalize our observations. The data presented in this paper require a more detailed theoretical understanding of the physio-chemical environment near nanoparticle surfaces such as aggregating SWCNTs.

1 Introduction

Additional control in directed and self-assembly of nanoscale elements should lead to more efficient and economically viable production of nanoscale sensors, switches, and actuators for mechanical and biological applications. Chemical functionalization can enhance integration of supramolecular and supraparticle assemblies for various technological enablers such as: metal catalysts for water purification, novel filter media and membrane coatings, or composite materials.[1] Better control over nanoparticle position, orientation, and topology should lead to optimized performance of new structural materials,[2, 3] organic carbon removal,[4-8] heavy metal removal,[9, 10] and antimicrobial systems.[11-16] An overview of supraparticle assemblies has been presented in a recent thematic issue of *Physical Chemistry Chemical Physics*.[17] The physics of supraparticle interactions differs from supramolecular interactions in the length scale governing the interactions. Amphiphilic molecules organize into supramolecular structures because of their complementary interactions with each other, and their entropic interactions with the solvent. Likewise amphiphilic hybrid-nanoparticles can assemble and form interesting multi-particle structures.[18-20]

Directed assembly of hybrid nanoparticles is illustrated in the electron micrograph shown in Fig. 1 (and Fig. S. 1-2 in the Electronic Supplementary Information). Here a multinuclear coordination complex[21] is mechanically wrapped about the ends of a dispersed single walled carbon nanotube (SWCNT).[22] After removal of unbound complex, citrate stabilized 15 nm colloidal Au nanoparticles (NPs) were titrated into the dispersion. This scanning electron microscopy (SEM) image clearly shows three Au NPs bound to the ends of each SWCNT. Without addition of the coordination complex, the Au NPs did not show preferential binding to the ends of the SWCNTs. There are three ~155 nm long SWCNTs between the sets of NPs,

yielding a hydrophilic-hydrophobic-hydrophilic motif. Better control over the lengths and diameters of the SWCNTs is required to enable the efficient synthesis of these amphiphilic hybrid nanoparticles. Controlled assembly of amphiphilic nanoparticles can lead to functional supraparticles such as nanoparticle micelles,[23] liposomes,[24] and nanostructured scaffolds.[25] Ultimately, better control of long range interactions (LRIs) between nanoparticles will enable higher fidelity in supraparticle synthesis. This paper aims to provide a better understanding of nanoparticle interactions that should lead to a rational design of supraparticles.

Current theory regarding LRIs in nanoscale science has been reviewed.[26] Measured and calculated optical spectra yield van der Waals-London Dispersion LRIs that result in subtle changes in the attractive Hamaker coefficients between SWCNTs.[27, 28] Universal graphitic potentials have been used to describe tube-tube attractive interactions[29] and cohesive energies of crossed perpendicular tubes have been measured to be ~50 kT.[30] Since SWCNT dispersions are kinetically stable,[31, 32] there must be a significant tube-tube repulsive barrier to overcome the cohesive forces upon tube-tube close contact. The precise nature of the repulsive barrier is not clear. Interaction potentials due to solvent organization about the SWCNTs[33, 34] and due to self-assembled surfactant organization about the SWCNTs[35] have been calculated. Surfactant mediated SWCNT dispersions can be more stable than pristine nanotubes due to structural forces contributed by the surface mediated organization of the surfactant.[36] However surface mediated structural organization of the solvent, can also enhance dispersion stability in nanostructured carbon systems.[37]

Our recent observations of “transient stability” during SWCNT aggregation in N-methyl-2-pyrrolidone (NMP) was ascribed to these organized solvent structural forces.[38] Interestingly, we did not observe these transient stabilities when the SWCNTs were dispersed in N,N-

dimethylformamide (DMF) which has similar properties to NMP. While NMP is a slightly better dispersant than DMF, the mixture of both solvents actually yields a more stable dispersion.[31] Moreover, the length of the observed "transient stability" was enhanced when the NMP dispersion was destabilized with divalent Ca^{2+} compared to monovalent Na^{1+} ions. The role of solvated ions on solvent structural repulsive interactions between SWCNTs requires more investigation. We have also shown that the critical coagulation concentration[38] (CCC) and the onset of aggregation[31] (X_o) of SWCNTs in aprotic polar solvents can be described by Derjaguin, Landau, Verwey, and Overbeek (DLVO)[39, 40] type interactions. DLVO type interactions have been used to describe the stability or aggregation of modified SWCNTs[41, 42] and multi-walled tubes[43-46] in aqueous media. However, the precise nature of the electrical double layer (EDL) repulsive barrier model for "pristine" SWCNTs in aprotic polar solvents is not clear.

The net repulsive barrier which enables pristine SWCNT stability in the aprotic polar solvents studied here is a summation of the LRIs such as van der Waals attraction, EDL repulsion, and the steric repulsion from tube-mediated structural forces of the layers of organized solvent between the nanotubes. The purpose of this work is to attempt to decouple the relative contributions of these two contributing forces using the kinetics of aggregation as a probe of dispersion stability. The results below describe the stability and aggregation kinetics of SWCNTs as a function of coagulant type, shape, charge, and ability to bind to the SWCNTs. We have used three classes of coagulants to probe different aspects of stability and aggregation. We use simple inorganic salts, mononuclear metal coordination complexes, and multinuclear metal coordination complexes in this study. The metal complexes can undergo charge transfer with the SWCNTs while the inorganic salts do not. The multinuclear metal complexes bind to the SWCNTs while the mononuclear complexes do not. The three dinuclear metal complexes have

similar chemical morphology and electronic properties but differ in their net charge (+2, +3, and +4). We have chosen this set of coagulants to try to decouple the various interactions between the coagulant, the particle, and the solvent. These kinetics data allow us to test stability and aggregation mechanisms. Specifically we compare the EDL model to the structured solvent layer model. Detailed kinetics data should help determine the nature of LRIs between dispersed nanoparticles in general. A full understanding of these interactions can enable rational design of supraparticle assemblies for functional materials.

2 Experimental

2.1 Sample Preparation

DMF (Fisher, Spectranalyzed) was used as purchased, and kept dry under an $N_{2(g)}$ blanket such that water contamination is below 1000 ppm. At this low level of water contaminant, LRI from hydration forces are insignificant, and not considered in this study. Single-walled carbon nanotubes were HiPCO (Grade P CNT from CNI, now Unidym, 0.8 – 1.2 nm diameter, 100 – 1000 nm length). SWCNT dispersions were prepared by adding powder (0.5 mg) to the DMF (20 mL) then tip ultrasonicated without temperature or gas environment regulation[47] for 30 min at 10 W RMS by a Fisher Scientific Sonic Dismembrator 60 (1/8" tip ultrasonicator). After ultrasonication, dispersions were ultracentrifuged with a Beckman Optima XL-100K at 20,000 g for 20 min to sediment any undispersed SWCNTs. The supernatant was carefully collected, then diluted to a final SWCNT concentration of ~10 mg L^{-1} and ultrasonicated for another 30 min to ensure excellent dispersion immediately before any coagulant was added. Dispersions typically had less than 1000 ppm of water as determined by H-NMR spectroscopy (Table S.1).

2.2 Aggregation Kinetics

Aggregation kinetics for SWCNT dispersions were performed by adding coagulant dissolved in DMF. All of the coagulants used completely dissociate in DMF, as confirmed by conductivity measurements with a Fisher Scientific Accumet AR20 at 25 °C. 1 mL samples for the aggregation studies were prepared by adding coagulant solution to SWCNT samples for a wide range of coagulant concentrations. The samples were allowed to incubate for 48 – 672 hours, because of the slow aggregation rates near the onset of aggregation. Each sample was then centrifuged at 10,000 g for 10 minutes in an Eppendorf 5415C tabletop centrifuge to sediment any aggregated SWCNTs. Supernatant (100 μL) was immediately transferred to a cuvette to measure the SWCNT concentration based on optical absorption.[48, 49] SWCNT concentrations were normalized to a control sample that did not have any coagulant added to it. At least three measurements were collected for each coagulant concentration.

2.3 Coagulants Used

Coagulants used in this study are best described by one of three categories. The inorganic salts, NaBr, $Ba(NO_3)_2$, $Ba(ClO_4)_2$, and $Al(NO_3)_3$, were used as purchased after they were dried in a vacuum oven. Mononuclear ruthenium coordination complexes, [Ru(1,10-phenanthroline-5,6-dione)(2,2';6',2"-terpyridine)Cl](PF_6)·(**+1 Ru1**) and [Ru(1,10-phenanthroline)$_3$]$(PF_6)_2$ (**+2 Ru1**) were both synthesized, purified and characterized using slight adaptations of previously reported methods.[50, 51] Multinuclear ruthenium coordination complexes, [Cl(2,2';6',2"-terpyridine)Ru(tetrapyrido[3,2-α:2′,3′-c:3″,2″-h:2″,3″-j]phenazine)Ru(2,2';6',2"-terpyridine)Cl]$(PF_6)_2$ (**+2 Ru2**), [(1,10-phenanthroline)$_2$Ru(tetrapyrido[3,2-α:2′,3′-c:3″,2″-h:2″,3″-j]phenazine)Ru(2,2';6',2"-terpyridine)Cl]$(PF_6)_3$ (**+3 Ru2**), and [(1,10-

phenanthroline)$_2$Ru(tetrapyrido[3,2-α:2′,3′-c:3″,2″-h:2″,3″-j]phenazine)Ru(1,10-phenanthroline)$_2$](PF$_6$)$_4$ (**+4 Ru2**) were all synthesized, purified and characterized using our previously reported methods[52] that will not be described here for brevity.

2.4 Zeta Potential

The electrophoretic mobility of the SWCNT dispersions was measured using a Brookhaven Instruments Corporation ZetaPALS system. The phase analysis light scattering technique is more sensitive to mobility measurements in organic solvents like DMF. Multiple runs are averaged. Zeta potentials are calculated using the Smoluchowski equation. Solutions were measured in glass cuvettes at 25.0 °C.

3 Results and Discussion

3.1 All coagulants are fully dissociated

Limiting molar conductivities Λ° of coagulants were determined by fitting Kohlrausch's law to measured conductivity data. These results are consistent with literature values for inorganic salts and listed in Table 1. Linear region of Kohlrausch's law for the ruthenium coordination complexes are shown in Fig. S. 3. Coagulant concentrations used in this study were 10^2 – 10^5 times more dilute than shown in the strong electrolyte conductance region. All of the coagulants used in this study are strong electrolytes and completely dissociate in DMF at the concentrations used. Conductivities of the pure solvents use here are below 1 uS/cm.

3.2 Zeta potential of SWCNT dispersions

The zeta potential on a particle is often used to characterize the strength of the EDL repulsion. There are many dispersion stability studies of carbon nanotubes in aqueous systems.[53, 54] The electrophoretic mobility of the dispersed particles is measured[42] and the zeta potential is calculated using a model. In general there is no valid model relating measured electrophoretic mobility (EPM) of a dispersed SWCNT to the electrostatic potential, the zeta potential, at the slipping plane of the diffuse layer. Typically the Smoluchowski approximation is used to account for the solvent's dielectric constant and viscosity and to calculate the zeta potential. Reported values of zeta on dispersed purified carbon nanotubes vary greatly from -5 mV to -70 mV.[54] The measured zeta can depend strongly on the solvent used in the dispersion. Kim et al. found the zeta of oxidized carbon nanotubes to be -10 mV to -20 mV in various alcohols and -60 mV in ethylene glycol.[55]

Our EPM and zeta results are consistent with those reported in the literature. Fig. S. 4 (in electronic Supplemental Materials) shows a stable zeta potential of freshly dispered SWCNTs in dry DMF of -47 mV. The zeta potential is reduced as we add coagulant, increasing the ionic strength in the dispersion. At 0.5 μM **+2Ru1**, the +2 mononuclear ruthenium complex, the zeta drops to -41 mV. When we increase the concentration of the coagulant to 1.0 μM the zeta drops further as expected for a colloidal dispersion as you approach the onset of aggregation (X_o = 1.98 ± 0.07 μM **+2Ru1**) indicating that the EDL repulsive potential is collapsing.

3.3 Diffusion Limited Aggregation

Using our previously reported sedimentation technique[38] we have studied the aggregation kinetics of SWCNTs in aprotic polar solvents due to coagulation induced by addition of inorganic salts. There are two time domains that interest us most. At high coagulant

concentrations we can determine the CCC, where the SWCNTs are aggregating near their diffusion limited rates.[38] Under these conditions the kinetics obey a DLVO type description where we can calculate an inverse stability ratio, 1/W, the diffusion limited colloid aggregation (DLCA) rate constant, and the CCC. In Fig. 2 we plot the concentration of SWCNTs left in the dispersion versus time given a fixed amount of NaBr in DMF added. Because the kinetics at these concentrations is so fast, the samples are spinning in a centrifuge during the aggregation process as described in our previous studies.[38] From the inverse stability ratio we derive a CCC of 1.3 ± 0.1 mM (result ± standard error). These data are well fit by a second order integrated rate law: $[SWCNT] = \frac{[SWCNT]_0}{1+ [SWCNT]_0 * k_d * t}$ yielding a diffusion limited rate constant k_d = 2.09 ± 0.06 $(mg/L)^{-1}min^{-1}$. Second order kinetics implies a simple two body attachment mechanism such as:

$$SWCNT + SWCNT \rightarrow SWCNT_2$$

$$SWCNT + SWCNT_x \rightarrow SWCNT_{x+1}$$

$$SWCNT_x + SWCNT_y \rightarrow SWCNT_{x+y},$$

resulting in a polydisperse distribution of aggregates.

Our studies of NaBr added to NMP dispersions of SWCNTs yielded a diffusion limited rate constant, k_d = 0.89 ± 0.07 $(mg/L)^{-1}min^{-1}$, which is a factor of 2.35 smaller than that in DMF. This result is consistent with the factor of 2.38 increase in the bulk viscosity of NMP over DMF (1.9 cP vs. 0.8 cP respectively at 25 °C) according to the Stokes – Einstein equation. Following the Smoluchowski formulism for quasi-perikinetic irreversible aggregation,[56] the particle-size-independent DLCA rate constant $k_d = 4k_bT/3\eta = 6 \cdot 10^{-18} \frac{m^3}{particle \cdot s}$ in NMP. Since we measured rates of mass loss and have a polydisperse system, we cannot accurately convert our measured k_d to units of $(m^3/particle \cdot s)$. Since we only remove bundled and aggregated tubes during the kinetics experiments, the actual mass of each particle is much larger than that of the

individual dispersed tubes so an absolute comparison of these rate constants is not possible. Using approximate average molar mass of SWCNTs (10^6 g/mol based on typical diameter and length distributions) and approximating the number of tubes, ~100 per aggregating bundle (as determined from 6 – 8 nm diameter bundles from SEM measurements of the aggregated material) our experimentally determined $k_d \simeq 10^{-18}\ \frac{m^3}{particle \cdot s}$ is consistent with that predicted by DLVO considerations. It is possible that solvent dynamics near the interacting nanotubes provides an additional kinetic barrier to aggregation even after the EDL is collapsed by the NaBr. The steric barrier from the tube-mediated solvent structure needs to be sheared off of the tubes as they come together and orient parallel to each other. It is possible that the higher bulk viscosity of the NMP also results in slower removal of the last solvent layer around the tube. This effect could be measured independently using a crossed-tube force measurement.[30]

Mac Kernan and Blau[33] calculated the free energy of interaction between SWCNTs in NMP as a function of torsion angle between contacting tubes. Due to the structural forces of the NMP bound to the SWCNT, the lowest barrier for tube-tube aggregation is when the tubes are crossed at 90°. The tubes must then diffuse radially over an ~8 kT barrier to reach their stable aligned state forming small bundles as observed. They predicted that this potential barrier should lead to experimentaly observable "dynamical transients." We have observed a "transient stability" in the aggregation kinetics of SWCNTs in NMP as reported previously.[38] The repulsive barrier between parrallel tubes is significantly higher than for perpendicularly crossed tubes, and SWCNTs always aggregate as bundles and ropes of parrallel tubes. Therefore, the rotational diffusion of the tubes coupled with the viscous flow of the solvent layer away from the interacting surfaces is likely involved in the observed kinetics of aggregation.

However, we do not observe a transient stability at high coagulant concentration where any EDL repulsion is minimized and the tube-mediated solvent structural forces should be the dominate stabilization mechanism. Moreover, we do not observe any transient stability from aggregating dispersions in pure DMF as shown in Fig. 2. This is curious given that the dispersion stability between NMP and DMF is very similar, as determined by the CCC (5.5 mM vs 1.3 mM respectively) , and the properties of the solvent are very similar (NMP/DMF: polarity 4.09 / 3.81 D, dielectric constant 32.2 / 37, density 1.028 / 0.944 g/L, surface tension 40.8 / 37.1 mN/m).

In Fig. 3 we analyze aggregation kinetics of dispersions in different solvent systems with NaBr as the coagulant. The data denoted by the square marks describes reaction limited colloid aggregation (RLCA) kinetics (1/W listed in legend) and the data denoted by the circle marks are near the DLCA regime (1/W = 0.3 for each). At high coagulant concentration, and high inverse stability ratio, the dispersions are near the CCC and aggregating without any transient stability. Data that does not exhibit a transient stability are fit by a 2nd order rate law as expected (solid line, all reduced chi squares are below 0.05, all adjusted $R^2 > 0.99$). As we described previously,[38] only samples that contain NMP exhibit any measurable transient stability. That is why we interpreted this observation as due to NMP structural forces keeping the tubes apart as predicted by molecular dynamics calculations.[33] Given our new observations, we are not convinced that tube-mediated solvent structure is the mechanism for transient stability. We have repeated Mac Kernan and Blau's molecular dynamics calculations[33] using the same COMPASS force field, ensemble, temperature, and method but replacing the NMP in their study with DMF (see S. 5 in electronic Supplemental Materials). We find that DMF forms the same tube-mediated solvent structure around and between the tubes as does the NMP in Mac Kernan and Blau's study as illustrated in Fig. S. 5. A recent molecular dynamics study of solvent structure

between graphene layers found that the potential of mean force (PMF) between the graphene sheets solvated by NMP[37] and DMF were nearly identical.[57] Since the properties of NMP and DMF are similar, and the PMF between nanostructured carbons is similar, and the transient stability disapears in the DLCA regime, it is unlikely that tube-mediate solvent structure is the mechanism for the observed transient stability. It may not even be the most dominate of the long range interactions under these conditions.

3.4 Dispersion Stability

We measured the CCC for NaBr in a NMP SWCNT dispersion, quiescent and in the dark, to be 5.5 ± 0.5 mM. This is consistent with similar studies of NaI in NMP during agitation by Frolov et al.[58] Their work reports a qualitative description of dispersion stability consistent with what we have reported quantitatively for the NaBr,[31] and other inorganic salts.[59] In this paper we quantify the dispersion stability, X_o, of SWCNTs in DMF and measure the slow RLCA kinetics for a homologous series of ruthenium complexes as a function of charge state and binding capabilities of the coagulant.

At very low coagulant concentration we measure SWCNT dispersion stability and aggregation kinetics. The onset of aggregation, as defined by X_o, is the concentration of coagulant that results in the aggregation of 50% of the SWCNTs after a fixed time interval. Integration of the Maxwell-Boltzmann distribution for energies greater than the EDL barrier yields a sigmoidal relationship that we describe using the simpler empirical relation:

$$\frac{[SWCNT]}{[SWCNT]_o} = \frac{A}{1+\exp\left[\frac{[coagulant]-X_o}{\Delta X}\right]} \qquad \text{(Eqn. 1)},$$

where $\frac{[SWCNT]}{[SWCNT]_o}$, is the fraction of SWCNTs remaining in dispersion which asymptotically approaches A at infinite dilution. The onset of aggregation, or dispersion stability, X_o and width, ΔX, of the sigmoidal function[31] are determined by fitting Eqn. 1 to the data as shown in Fig. 4. At very low concentrations of coagulant the SWCNT dispersion is stable for months. In Fig. 4 we show how the SWCNTs aggregate after 48 h, quiescent and in the dark, as the concentration of the **+1Ru1** coagulant increases. We have shown previously that the dispersion stability in the RLCA regime and the CCC in the DLCA regime depends on the properties of the solvent.[31, 38]

In this study we focus on the dispersion stability of the SWCNTs as we change the chemical properties of the coagulant. According to DLVO theory, the collapse of the EDL depends on the charge state of the ions in solution.[39, 40] For the cation charge state $Z_+ = +1$ of NaBr in DMF, the measured dispersion stability is $X_o = 150 \pm 20$ μM after 48 h in the dark. We studied two inorganic salt coagulants with $Z_+ = +2$. Both $Ba(NO_3)_2$ and $Ba(ClO_4)_2$ in DMF had similar onsets of aggregation 3.99 ± 0.16 μM and 3.65 ± 0.12 μM respectively after 48 h in the dark. The nature of the coagulant's anion does not affect the dispersion stability. Moreover, the dispersion stability is nearly independent of SWCNT concentration from 3 mg/L to 30 mg/L consistent with an RLCA mechanism. We also studied a third inorganic salt, $Al(NO_3)_3$ in DMF. With $Z_+ = +3$ for the solvated Al^{3+} cation the dispersion stability dropped to 1.46 ± 0.028 μM. According to DLVO theory for a lyophobic particle that obeys the Langmuir approximation in which the coagulant does not bind to the particle, the CCC should scale as Z_+^{-6}. However, when the zeta potential drops linearly with the concentration of the coagulant concentration the Debye-Huckle approximation predicts a CCC dependence on Z_+^{-2}. For the four different inorganic salts we studied the slope of the observed Schulze-Hardy plot $\log(X_o)$ vs. $\log(Z_+)$is -4.4 ± 0.4 as shown in Fig. S. 6 (Electronic Supplementary Information). The second class of coagulants we

studied are mononuclear ruthenium complexes **+1Ru1** with $Z_+ = +1$ and **+2Ru1** with $Z_+ = +2$. The slope of the Schulze-Hardy plot reduced slightly to -4.0 ± 0.7.

While the slopes are similar for these different classes of coagulants, we find that there are significant differences in X_o as the size of the solvated ion is varied. For the $Z_+ = +1$ cations the dispersion stability drops from $X_o = 150 \pm 6$ μM for Na^+ down to $X_o = 49.7 \pm 0.5$ μM for the **+1Ru1** cation with a PF_6^- anion. Measured solvation number of Na^+ is 3.3 in DMF[60] and 5.2 in NMP[58] with a solvated radius of < 0.5 nm. The much larger **+1Ru1** cation has a calculated coordination number of DMF ~20 with a solvated radius of ~11 nm as shown in Fig. S. 7 (electronic Supplemental Materials). Since the free energy of solvation goes down as the solvation sphere radius increases,[61] the **+1Ru1** cation can more easily make a direct contact with the surface of the SWCNT. The ion-tube contact should be more effective at lowering the zeta potential and thereby destabilizing the dispersion resulting in a lower X_o.

We observe similar results from the $Z_+ = +2$ and $Z_+ = +3$ cations. The Ba^{2+} inorganic salt yielded a $X_o = 4.0 \pm 0.1$ μM where the mononuclear **+2Ru1** cation yielded a $X_o = 1.98 \pm 0.07$ μM and the larger dinuclear **+2Ru2** cation yielded a $X_o = 1.22 \pm 0.02$ μM. Also, the Al^{3+} inorganic salt yielded a $X_o = 1.46 \pm 0.03$ μM while the +3 cation of the dinuclear **+3Ru2** salt yielded a significantly smaller $X_o = 0.37 \pm 0.01$ μM. These trends are consistent with an ion's ability to disrupt the solvent shell around the SWCNTs and collapse the EDL repulsion leading to aggregation. While the data show a correlation between solvated ion size and dispersion stability, more theoretical work is needed to support a valid mechanism that explains these data.

It may be that the lower dispersion stability of the +2 dinuclear complex as compared to the +2 mononuclear complex is a simple matter of charge density on the solvated cation. However, the multinuclear complexes seem to destabilize the dispersions differently than the

mononuclear complexes or the inorganic salts. The Schultz-Hardy plot for the multinuclear complexes is shown in Fig. 5. There are two limiting cases for destabilization of the EDL. The magenta line predicts $\log(X_o)$ vs. $\log(Z_+)$ for asymmetric coagulants (i.e., of the form MX_y) that do not affect the surface potential on the SWCNTs (Langmuir approximation) and the blue line for asymmetric coagulants that reduced the zeta potential linearly with the concentration of the coagulant (Debye-Huckle approximation). These measured X_o data exhibit a slope = -2.30 ± 0.13 (black line) which indicates that these coagulants are contacting and possibly binding to the SWCNTs. This behavior is significantly different than that of the mononuclear complexes and inorganic salts. A geometry optimized DFT (BLYP) model of the **+4Ru2** cation bound to a (10,0) SWCNT is shown in the inset of Fig. 5. The bridging ligand of the dinuclear complex distorts and wraps around the tube upon binding. We have measured the Langmuir adsorption isotherms and used isothermal titration calorimetry to show that these dinuclear complexes bind strongly to SWCNTs and the binding affinity increases with cation charge state.[62] Moreover, the mononuclear species do not bind strongly and the **+1Ru1** cation does not seem to bind at all. From conductivity measurements we find that the inorganic salts in this study do not bind to the SWCNTs. The conductivity of the supernatant from dispersion is the same after aggregated tubes are removed. It appears that the ability of the multinuclear complexes to bind to the SWCNTs changes the mechanism of aggregation.

3.5 Reaction Limited Aggregation Kinetics

The reaction limited aggregation kinetics of SWCNT aggregation at low coagulant concentration was also measured as a function of coagulant type, shape, charge, and ability to bind to the SWCNTs. In Fig. 6 we show dispersion stability data after different incubation times of

quiescent dispersions in the dark. These data are fit by the sigmoidal function described above from 48 to 672 h after the coagulant was added. The curves shift to lower X_o with longer incubation times as expected for a kinetically stable system.

The concentration of SWCNTs remaining versus time for a constant **+2Ru1** coagulant concentration is shown in Fig 6C. These data are fit by the two parameter 2nd order rate law shown above. While the initial concentration of the SWCNT dispersion for all of the experiments was 10 mg/L, the parameters $[SWCNT]_o$ and the rate constant k were not constrained. For all coagulants, $[SWCNT]_o$ extracted from the model are significantly lower than the actual initial concentration of the dispersion. There appears to be a fast kinetic process described by a larger initial rate constant. The concentration of coagulant used for the dispersion stability studies is much lower than those used to determine the true CCC. Other kinetic models were tested against these data. The zeroth order, two parameter, rate law is graphed and compared to the 2nd order rate law for several coagulants in Fig. S. 8 and all fitted parameters are listed in Table S. 2. For the NaBr, **+1Ru1**, and **+2Ru1** coagulants the 2nd order model has significantly smaller residual sum of squares (RSS). According to the Akaike's Information Criterion test,[63] the 2nd order model is 10^7 times more likely correct than the zeroth order model for the **+2Ru2** coagulant. The kinetic data for the **+3Ru2** and **+4Ru2** coagulant do not vary enough to statistically differentiate between zeroth order and second order mechanisms; nor do either model fit the data well.

While the CCC is the true onset of DLCA we find that the dispersion stability X_o is more useful to gauge how well a dispersion can withstand changes of ionic strength at very low coagulant concentrations. Moreover, X_o as a measure of intertube interaction potentials is pertinent to directed assembly strategies. We have shown that the CCC in mixed solvents of

DMF/NMP is intermediate to that of the pure solvents DMF or NMP alone.[38] However, the dispersion stability is affected more by the thermodynamics of the solvent. We found that there is a significantly enhanced dispersion stability in mixed solvents, like DMF/NMP, due to the optimization of the dispersive Hansen solubility parameter, and thereby lowering the attractive LRI between the SWCNTs.[31] Therefore, the dispersion stability is a better probe of the RLCA mechanism. In Fig. 7(A-C) we show the dispersion stability data for the three dinuclear coagulants, **+2Ru2**, **+3Ru2**, and **+4Ru2**. For ease of comparison, the range of the abscissa on Fig. 7(A-C) is kept constant (2 orders of magnitude). For the **+2Ru1** (Fig. 6B) and **+2Ru2** data it is clear that X_o decreases as the incubation time increases, as expected for RLCA behavior. However, the decrease in X_o for the **+3Ru2** coagulant is much smaller and X_o does not change, over the 672 hours studied, for the **+4Ru2** coagulant. These data are summarized in Fig. 7D where X_o is plotted versus time and fit to a linear relationship. The slope ± standard error from these data is listed in Table 2.

3.6 Ion-tube interactions: destabilizing the repulsive barrier

As discussed above, the dinuclear species binds to the SWCNTs. Moreover we have shown previously that the multinuclear complexes mechanically wrap around the SWCNTs as observed by UV-Vis and Raman spectroscopy; AFM, and DFT calculations.[22] As the **+4Ru2** complex binds to the SWCNTs during aggregation, the ionic strength of the solution will go down. Future studies of coagulant concentration versus time are needed to fully understand the slow aggregation by these multinuclear coagulants. The data in Table S2 suggest that after a fast kinetic process the aggregation of SWCNTs is not a simple process. We have also shown that the binding affinity, from our Langmuir adsorption isotherms, increases as the charge state on the

dinuclear complex increases such that, K_L = 1.09, 2.18, and 6.85 for the +2, +3, +4 complexes respectively.[62] In fact, the SWCNTs continue to follow a second order aggregation mechanism with the **+2Ru2** coagulant, as discussed above, where the **+3Ru2** and **+4Ru2** coagulants do not.

Frolov et al. reported a molecular dynamics study of the salt effects on SWCNT dispersions.[58, 61] However, their theoretical results do not explain our observations. Firstly their simulations used a very high concentration of ions. Since the measured CCC of NaBr in NMP is 5.5 mM there would only be one ion pair in their simulation box (7.50 x 7.50 x 5.19 = 292 nm^3) during rapid aggregation. Even more challenging is that we observe the onset of aggregation in NMP with a NaBr concentration of only X_o = 150 μM which would require a simulation box ~400 times larger just to put in one ion pair (the 50 μM H_2O in all samples would have to be considered too). Their simulation would then have over 60,000 NMP molecules and would be computationally challenging. This issue is exaserbated for the higher valence coagulants that we study. It may be impossible to properly model the effect of the **+4Ru2** at X_o = 0.137 μM with current methods. Yet, this low concentration of coagulant does destabalize the dispersion as we have shown here.

If the steric barrier from the tube-mediated solvent structure is the dominant source of dispersion stability, we must rationalize how the addition of ions results in the observed aggregation kinetics. Frolov et al. argue that the addition of salt increases the chemical potential of the SWCNTs making them more solvophobic.[61] Using the Kirkwood-Buff theory for hydrophobic systems in water,[64] they use Gibbs-Duhem equation to relate the change in the chemical potential of the SWCNT $\Delta\mu_{SWCNT} = -\Gamma \cdot \Delta\mu_{coagulant}$ to the change in the chemical potential of the coagulant by calculating Γ, the SWCNT-coagulant preferential interaction coefficient. For low salt concentrations they linearize this relationship to show the SWCNT's

chemical potential changes linearly with the mole fraction of coagulant added, $\Delta\mu_{SWCNT} \approx -k_bT \cdot C \cdot x_{coagulant}$. The constant C is a negative for small ions like Na^+ and I^- as determined from the radial distribution function (RDF) near the SWCNT surface when the ions are depleted from the near surface region. They calculate that $\Delta\mu_{SWCNT}$ is 0.23 k_bT/nm^2 when the NaI concentration is 0.15 M, and only 0.013 k_bT/nm^2 when the NaI concentration, in NMP, is 0.01 M. We have determined that a dispersion of SWCNTs in NMP is destabilized at a NaBr concentration of only 150 μM which would yield a $\Delta\mu_{SWCNT} \approx 5x10^{-6}$ k_bT/nm^2. While the thermodynamics of adding salt at high enough concentration can affect the SWCNT's solvophobicity, our system become unstable at far lower salt concentrations. Moreover, we find that the coordination complexes, especially the multinuclear species, actually bind to the SWCNTs which would yield a positive preferential interaction coefficient (C > 0) and make the SWCNTs *less* solvophobic, which is not observed. Additionally, the solvophobicity they derive is linear with salt concentration whereas we show a dispersion stability that decreases sigmoidally as we predicted by simple Maxwell-Boltzmann and EDL potential arguments above.

4 Conclusions

We have presented a comprehensive study of the stability and aggregation kinetics of SWCNT dispersions in two different aprotic polar solvents and by several couagulants. By changing the coagulant's concentration, charge, size, shape, and binding capability we measured both the dispersion stability and probed the mechanism for SWCNT aggregation. We focused our experiments on the fast kinetics DLCA regime and the slow kinetics of the RLCA regime. Our goal of this study was to try to elucidate the relative contributions of different interaction potentials that affect dispersion stability and aggregation. The three dominant interpartical interactions for these systems are the attractive van der Waals type potential, the repulsive tube

mediated solvent structural potential, and the DLVO type EDL repulsion. Clearly the attractive potentials have been most extensively studied and are consistent with direct experimental data. The attempt to model the structured solvent PMF by molecular dynamics is helpful, but not yet complete for more realistic systems.

Our data support that the DLVO type EDL interactions are the dominant LRI that stabilizes SWCNTs in non-aqueous solvents like NMP and DMF. An accurate theoretical description of the detailed nature of this EDL, specific to crossed tube-tube interactions in structured solvent environments is needed before addition kinetic mechanisms can be tested.[41, 65] There seems to be some contribution from ionic coagulants disrupting the tube-mediated solvent structure. It may be that this effect can explain the "transient stability" that we have reported previously. Our detailed kinetic study presented above does not support a mechanism based solely on structured solvent steric stabilization. Future experiments will measure coagulant concentration as a function of time to decouple the slow kinetics using larger coagulants that bind to the SWCNTs. Additional zeta potential measurements at longer times will aid the theoretic understanding of the EDL repulsive mechanism. In addition the use of different types of SWCNTs, with different amounts of oxidation will change the initial zeta on the particles and enable a kinetics study as a function of surface potential. Variable temperature studies could lead to an Arrhenius analysis of the intertube potential as a function of coagulant type and concentration. In so much that we can understand the tube-solvent-coagulant-tube interactions, we may be able to rationally design conditions that favor specific directed assembly motifs of connected nanoparticles; to design supraparticle assemblies.

5 Acknowledgements

The authors wish to thank Dr. Cliff Carlin for his help with the NMR measurement of water in DMF. Acknowledgement is made to the Donors of the American Chemical Society Petroleum Research Fund for partial support of this research. Acknowledgement is made to the Research Corporation and the NSF (Grant # 0404193) for partial support of this research. Financial support from Nanoscale Science Ph.D. program, the Center for Optoelectronics and Optical Communications at UNC Charlotte, and the Thomas Walsh Tuition Fellowship is appreciated.

References

1. M. A. C. Stuart, W. T. S. Huck, J. Genzer, M. Muller, C. Ober, M. Stamm, G. B. Sukhorukov, I. Szleifer, V. V. Tsukruk, M. Urban, F. Winnik, S. Zauscher, I. Luzinov and S. Minko, *Nature Materials*, 2010, **9**, 101-113.

2. B. S. Shim, Z. Y. Tang, M. P. Morabito, A. Agarwal, H. P. Hong and N. A. Kotov, *Chemistry of Materials*, 2007, **19**, 5467-5474.

3. Y. H. Hu, O. A. Shenderova, Z. Hu, C. W. Padgett and D. W. Brenner, *Reports on Progress in Physics*, 2006, **69**, 1847-1895.

4. H. T. Wang, A. A. Keller and F. T. Li, *Journal of Environmental Engineering-Asce*, 2010, **136**, 1075-1081.

5. L. Mahdavian and M. Raouf, *Integrated Ferroelectrics*, 2010, **114**, 7-16.

6. S. J. Zhang, T. Shao, H. S. Kose and T. Karanfil, *Environmental Science & Technology*, 2010, **44**, 6377-6383.

7. L. L. Ji, W. Chen, L. Duan and D. Q. Zhu, *Environmental Science & Technology*, 2009, **43**, 2322-2327.

8. S. B. Fagan, A. G. Souza, J. O. G. Lima, J. Mendes, O. P. Ferreira, I. O. Mazali, O. L. Alves and M. S. Dresselhaus, *Nano Letters*, 2004, **4**, 1285-1288.

9. X. S. Wang, J. J. Ren, H. J. Lu, L. Zhu, F. Liu, Q. Q. Zhang and J. Xie, *Clean-Soil Air Water*, 2010, **38**, 1131-1136.

10. A. M. Bond, W. J. Miao and C. L. Raston, *Langmuir*, 2000, **16**, 6004-6012.

11. S. Aslan, C. Z. Loebick, S. Kang, M. Elimelech, L. D. Pfefferle and P. R. Van Tassel, *Nanoscale*, 2010, **2**, 1789-1794.

12. A. S. Brady-Estevez, M. H. Schnoor, S. Kang and M. Elimelech, *Langmuir*, 2010, **26**, 19153-19158.

13. S. Kang, M. S. Mauter and M. Elimelech, *Environmental Science & Technology*, 2009, **43**, 2648-2653.

14. S. Kang, M. Pinault, L. D. Pfefferle and M. Elimelech, *Langmuir*, 2007, **23**, 8670-8673.

15. K. Saeed, *Journal of the Chemical Society of Pakistan*, 2010, **32**, 559-564.

16. N. Duran, P. D. Marcato, G. I. H. De Souza, O. L. Alves and E. Esposito, *Journal of Biomedical Nanotechnology*, 2007, **3**, 203-208.

17. D. Wang, *PCCP Phys. Chem. Chem. Phys.*, 2010, **12**, 11819-11820.

18. A. Baskin, W.-Y. Lo and P. Král, *ACS Nano*, 2012, **6**, 6083-6090.

19. T. Harada, F. Simeon, J. B. Vander Sande and T. A. Hatton, *PCCP Phys. Chem. Chem. Phys.*, 2010, **12**, 11938-11943.

20. R.-Y. Wang, H. Wang, X. Wu, Y. Ji, P. Wang, Y. Qu and T.-S. Chung, *Soft Matter*, 2011, **7**, 8370-8375.

21. F. M. MacDonnell, M. J. Kim and S. Bodige, *Coord. Chem. Rev.*, 1999, **186**, 535-549.

22. H. Chaturvedi, A. N. Giordano, M.-J. Kim, F. M. MacDonnell, S. S. Subaran and J. C. Poler, *J. Phys. Chem. C*, 2009, **113**, 11254-11261.

23. X. Sun, W. Huang, Y. Zhou and D. Yan, *PCCP Phys. Chem. Chem. Phys.*, 2010, **12**, 11948-11953.

24. C. S. Wagner, A. Fortini, E. Hofmann, T. Lunkenbein, M. Schmidt and A. Wittemann, *Soft Matter*, 2012, **8**, 1928-1933.

25. E. W. Edwards, D. Wang and H. Möhwald, *Macromolecular Chemistry and Physics*, 2007, **208**, 439-445.

26. R. H. French, V. A. Parsegian, R. Podgornik, R. F. Rajter, A. Jagota, J. Luo, D. Asthagiri, M. K. Chaudhury, Y.-m. Chiang, S. Granick, S. Kalinin, M. Kardar, R. Kjellander, D. C. Langreth, J. Lewis, S. Lustig, D. Wesolowski, J. S. Wettlaufer, W.-Y. Ching, M. Finnis, F. Houlihan, O. A. von Lilienfeld, C. J. van Oss and T. Zemb, *Reviews of Modern Physics*, 2010, **82**, 1887-1944.

27. R. Rajter and R. H. French, *International Journal of Materials Research*, 2010, **101**, 27-42.

28. R. F. Rajter, R. H. French, W. Y. Ching, W. C. Carter and Y. M. Chiang, *J. Appl. Phys.*, 2007, **101**, 054303.

29. L. A. Girifalco, M. Hodak and R. S. Lee, *Phys. Rev. B*, 2000, **62**, 13104-13110.

30. B. Bhushan and X. Ling, *Phys. Rev. B*, 2008, **78**, 045429.

31. M. W. Forney and J. C. Poler, *The Journal of Physical Chemistry C*, 2011, **115**, 10531-10536.

32. S. Giordani, S. D. Bergin, V. Nicolosi, S. Lebedkin, M. M. Kappes, W. J. Blau and J. N. Coleman, *J. Phys. Chem. B*, 2006, **110**, 15708-15718.

33. D. Mac Kernan and W. J. Blau, *Epl*, 2008, **83**.

34. J. H. Walther, R. L. Jaffe, E. M. Kotsalis, T. Werder, T. Halicioglu and P. Koumoutsakos, *Carbon*, 2004, **42**, 1185-1194.

35. P. Angelikopoulos, S. Al Harthy and H. Bock, *The Journal of Physical Chemistry B*, 2009, **113**, 13817-13824.

36. P. Angelikopoulos and H. Bock, *PCCP Phys. Chem. Chem. Phys.*, 2012, **14**, 9546-9557.

37. C. Fu and X. Yang, *Carbon*, 2013, **55**, 350-360.

38. M. W. Forney, J. S. Anderson, A. L. Ameen and J. C. Poler, *The Journal of Physical Chemistry C*, 2011, **115**, 23267-23272.

39. B. V. Derjaguin and L. Landau, *Acta Phys. Chim. URSS*, 1941, **14**, 633-662.

40. E. J. W. Verwey and J. T. G. Overbeek, *Theory of the stability of lyophobic colloids*, Elsevier, Amsterdam, 1948.

41. L. Wu, B. Gao, Y. Tian, R. Muñoz-Carpena and K. J. Zigler, *Langmuir*, 2013, **29**, 3976-3988.

42. D. P. Jaisi, N. B. Saleh, R. E. Blake and M. Elimelech, *Environmental Science & Technology*, 2008, **42**, 8317-8323.

43. A. R. Petosa, D. P. Jaisi, I. R. Quevedo, M. Elimelech and N. Tufenkji, *Environmental Science & Technology*, 2010, **44**, 6532-6549.

44. E. Heister, C. Lamprecht, V. Neves, C. Tîlmaciu, L. Datas, E. Flahaut, B. Soula, P. Hinterdorfer, H. M. Coley, S. R. P. Silva and J. McFadden, *ACS Nano*, 2010, **4**, 2615-2626.

45. B. Smith, K. Wepasnick, K. E. Schrote, A. R. Bertele, W. P. Ball, C. O'Melia and D. H. Fairbrother, *Environmental Science & Technology*, 2008, **43**, 819-825.

46. P. Yi and K. L. Chen, *Langmuir*, 2011, **27**, 3588-3599.

47. M. W. Forney and J. C. Poler, *J. Am. Chem. Soc.*, 2010, **132**, 791-797.

48. A. N. Giordano, H. Chaturvedi and J. C. Poler, *J. Phys. Chem. C*, 2007, **111**, 11583-11589.

49. J. L. Bahr, E. T. Mickelson, M. J. Bronikowski, R. E. Smalley and J. M. Tour, *Chem. Comm.*, 2001, 193-194.

50. T. Fujihara, R. Okamura, T. Wada and K. Tanaka, *Dalton Transactions*, 2003, 3221-3226.

51. C. Hiort, P. Lincoln and B. Norden, *J. Am. Chem. Soc.*, 1993, **115**, 3448-3454.

52. J. R. Alston, S. Kobayashi, T. J. Younts and J. C. Poler, *Polyhedron*, 2010, **29**, 2696 - 2702.

53. L. Jeongwoo, K. Myunghun, H. Chang Kook and S. Sang Eun, *Measurement Science and Technology*, 2007, **18**, 3707.

54. H. Hu, A. P. Yu, E. Kim, B. Zhao, M. E. Itkis, E. Bekyarova and R. C. Haddon, *J. Phys. Chem. B*, 2005, **109**, 11520-11524.

55. D. H. Kim, Y. S. Yun and H.-J. Jin, *Current Applied Physics*, 2012, **12**, 637-642.

56. M. von Smoluchowski, *Zeitschrift Fur Physikalische Chemie--Stochiometrie Und Verwandtschaftslehre*, 1917, **92**, 129-168.

57. C.-J. Shih, S. Lin, M. S. Strano and D. Blankschtein, *J. Am. Chem. Soc.*, 2010, **132**, 14638-14648.

58. A. I. Frolov, R. N. Arif, M. Kolar, A. O. Romanova, M. V. Fedorov and A. G. Rozhin, *Chemical Science*, 2012, **3**, 541-548.

59. A. N. Giordano, H. Chaturvedi and J. C. Poler, *J. Phys. Chem. C*, 2007, **111**, 11583-11589.

60. H. Ohtaki, *Pure and Applied Chemistry*, 1987, **59**, 1143-1150.

61. A. I. Frolov, A. G. Rozhin and M. V. Fedorov, *ChemPhysChem*, 2010, **11**, 2612-2616.

62. J. R. Alston and J. C. Poler, in *Mater. Res. Soc. Symp. Proc.*, Editon edn., 2011, vol. 1303, pp. 185 - 191.

63. H. Bozdogan, *Psychometrika*, 1987, **52**, 345-370.

64. S. Pal and F. Müller-Plathe, *The Journal of Physical Chemistry B*, 2005, **109**, 6405-6415.

65. E. G. Pogorelov, A. I. Zhbanov, Y.-C. Chang and S. Yang, *Langmuir*, 2011, **28**, 1276-1282.

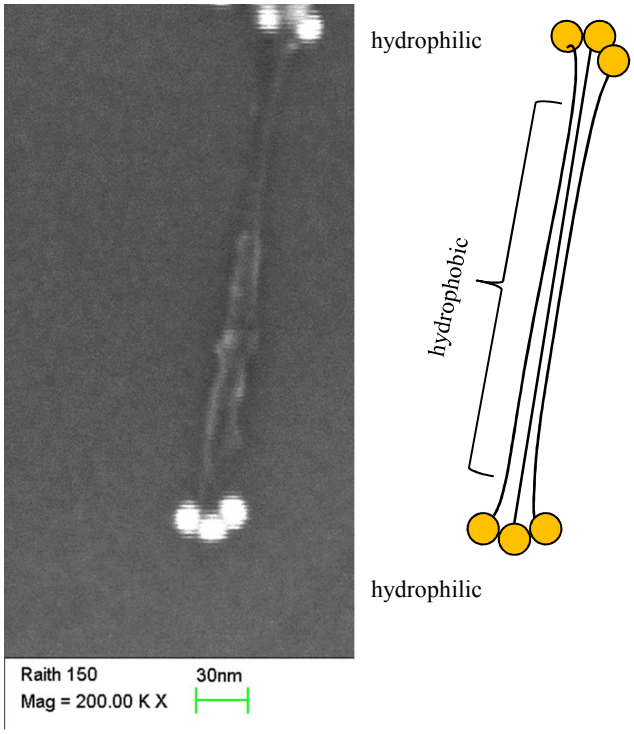

Fig. 1 SEM of hybrid supraparticle assembly (Au-SWCNT-Au). Cartoon of model shown at right. (see Fig. S. 1-2 in the Electronic Supplementary Information for experimental details)

Table 1. Limiting molar conductivities and 48 h dispersion stability in DMF at 25 °C

Species	$\Lambda°$ (S cm^2/mol)	Z_+	X_o (μM)
[1]NaBr	59	+1	150 ± 6
[2]$Ba(ClO_4)_2$	181	+2	4.0 ± 0.1
$Al(NO_3)_3$	213	+3	1.46 ± 0.03
+1 Ru1	60	+1	49.7 ± 0.5
+2 Ru1	156	+2	1.98 ± 0.07
+2 Ru2	170	+2	1.22 ± 0.02
+3 Ru2	224	+3	0.37 ± 0.01
+4 Ru2	346	+4	0.137 ± 0.003

(1) Pistola, G.; Pecol, G.; Scrosati, B. *La Rioerca scientifica* **1967**, *37*, 1167.
(2) Prue, J. E.; Sherrington, P. J. *Trans. Faraday Soc.* **1961**, *57*, 1795.

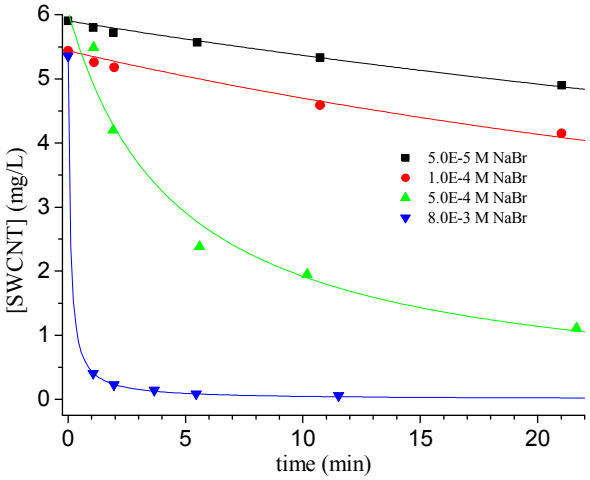

Fig. 2 Kinetics of SWCNT aggregation near the DLCA regime. Data is fit with a second order integrated rate law. SWCNTs are aggregating while under 10,000 g in a centrifuge.

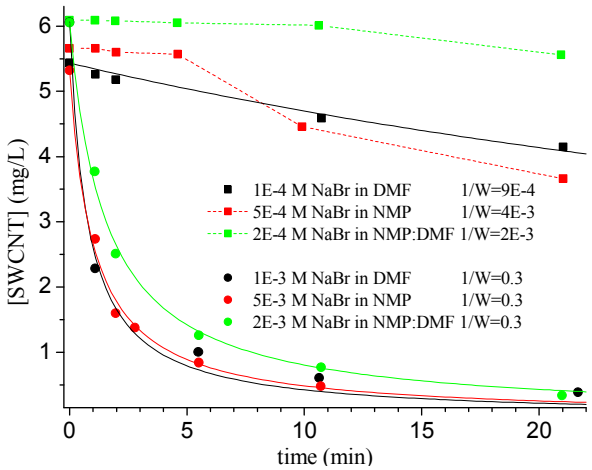

Fig. 3 Kinetics of SWCNT aggregation in the solvents pure DMF (black), pure NMP (red), and 50:50 NMP:DMF (green). Square symbols are for RLCA regime and circle symbols are for DLCA regime. Transient stability is denoted by dashed line to aid the eye. Solid lines are 2nd order rate law fits to the data.

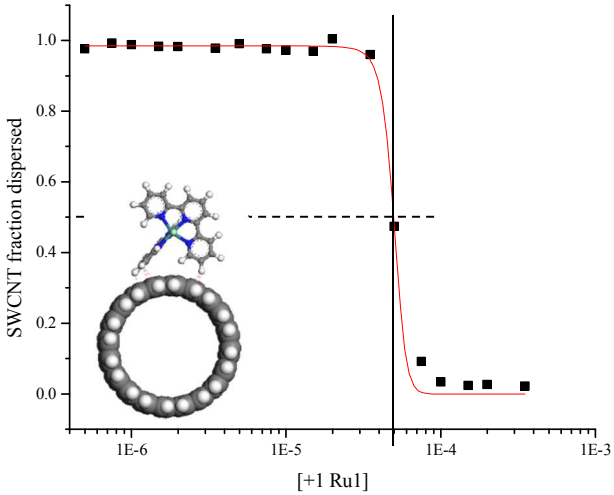

Fig. 4 Dispersion Stability of SWCNT aggregation near the RLCA regime. X_o is the concentration of the **+1Ru1** coagulant as determined from the fit of the data where 50% of the SWCNTs have aggregated after 48 h in the dark. Inset shows **+1Ru1** near a SWCNT (edge view)

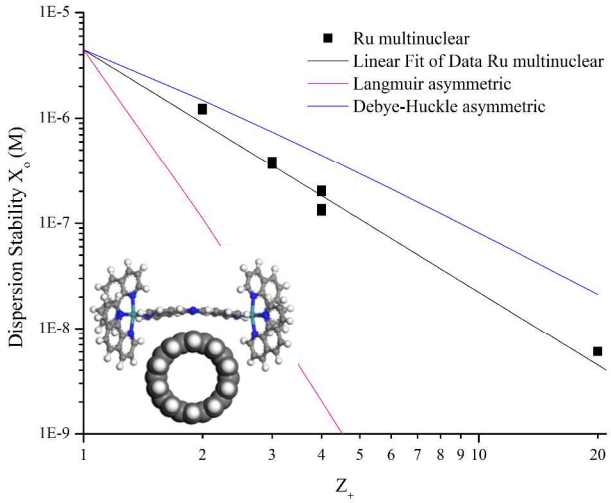

Fig. 5 Schulze-Hardy plot of dispersion stability versus charge on coagulant's cation. Multinuclear ruthenium complexes (black square) with a slope = -2.30 ± 0.13 indicating low surface potential on SWCNTs. Predicted lines for asymmetric coagulants, under Debye-Huckle approximation (blue line) and Langmuir approximation (magenta line), show limiting behavior.

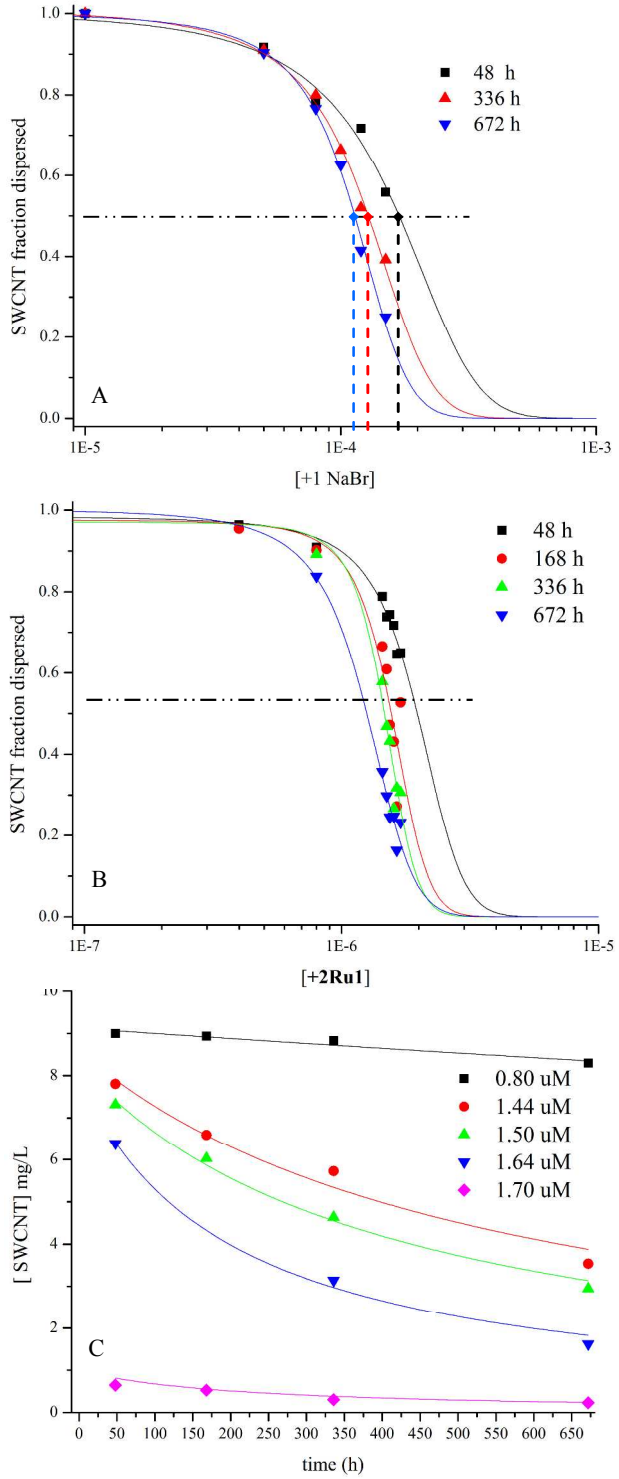

Fig. 6 Dispersion stability data of SWCNTs in DMF with NaBr (A) and **+2Ru1** (B) coagulants show X_o decreasing as time increases. (vertical dashed lines). These data are also plotted as SWCNT concentration versus time for five different concentrations of **+2Ru1** (C). RLCA kinetics data in (C) are described by a second order rate law in [SWCNT].

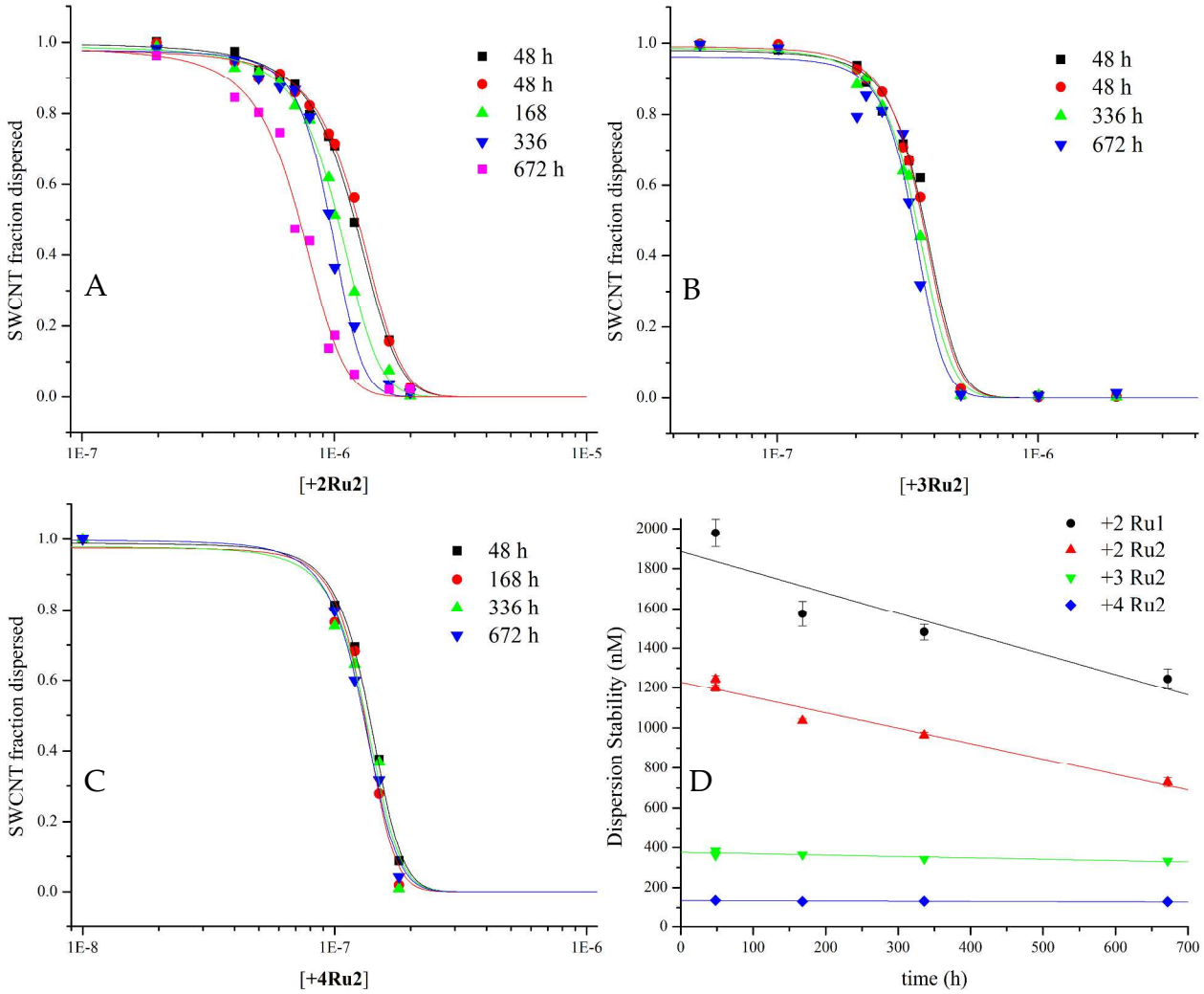

Fig. 7 Dispersion stability data for various coagulants, **+2Ru2** (A), **+3Ru2** (B), and **+4Ru2** (C) in DMF as a function of incubation time. X_o vs t is plotted in (D) and fit with a linear relationship.

Table 2. Slope of X_o vs. time

Species	$\Delta X_o/\Delta t$ (nM/h)
NaBr	-48 ± 30
+2 Ru1	-1.03 ± 0.32
+2 Ru2	-0.77 ± 0.09
+3 Ru2	-0.070 ±0.018
+4 Ru2	-0.0098 ± 0.005